Journal of Power Sources 196 (2011) 7404–7410

Contents lists available at ScienceDirect

Journal of Power Sources

journal homepage: www.elsevier.com/locate/jpowsour

A novel CuFe-based catalyst for the oxygen reduction reaction in alkaline media

Qinggang He[a], Xiaofang Yang[b], Xiaoming Ren[c], Bruce E. Koel[b], Nagappan Ramaswamy[d], Sanjeev Mukerjee[d], Robert Kostecki[a,*]

[a] Lawrence Berkeley National Laboratory, Environmental Energy Technology Division, 1 Cyclotron Road, Berkeley, CA 94720, USA
[b] Department of Chemistry and Center for Advanced Materials and Nanotechnology, Lehigh University, Bethlehem, PA 18015, USA
[c] U.S. Army Research Laboratory, 2800 Powder Mill Rd., RDRL-SED-C, Adelphi, MD 20783, USA
[d] Department of Chemistry and Chemical Biology, Northeastern University, 360 Huntington Avenue, Boston, MA 02115, USA

ARTICLE INFO

Article history:
Received 9 February 2011
Received in revised form 6 April 2011
Accepted 6 April 2011
Available online 17 April 2011

Keywords:
Alkaline fuel cell
Oxygen reduction reaction
Non-noble electrocatalyst
CuFe

ABSTRACT

The primary objective of this work is to develop alternative electrocatalysts to Pt-based materials for the oxygen reduction reaction (ORR) in alkaline fuel cells. We synthesized a bicore CuFe/C composite electrocatalyst by impregnation of iron and copper phthalocyanine-based complexes into a carbon support, followed by pyrolysis at 800–900 °C in an Ar atmosphere. This novel composite catalyst exhibits electrochemical performance for ORR in 0.1 M KOH similar to a commercial Pt/C (BASF Fuel Cell, 30%) catalyst at 6-fold lower CuFe loading. High resolution X-ray photoelectron spectroscopy (HR-XPS) results indicate that coordination bonding between Fe and N atoms still remains and show that a mixed Cu(I)/Cu(II) valency exists in the CuFe/C catalyst after high temperature heat treatment. The Cu(I)/Cu(II) redox mediator adjacent to Fe atoms is crucial to provide electrons to the $N_xFe–O_2$ adduct and maximize the overall rate of the reduction reaction. The results of this study may offer a new approach to development of efficient catalysts for oxygen reduction to water in alkaline media.

1. Introduction

Alkaline fuel cells (AFCs) were one of the first fuel cell technologies developed and they have demonstrated efficiencies near 60% in space applications. Unfortunately, the inherent low power density and electrolyte poisoning by CO_2 [1–3] added to the relatively high cost of AFCs and led to the rapid growth of acidic analogs such as the proton exchange membrane fuel cells (PEMFCs). On the other hand, the fast kinetics of alcohol oxidation in alkaline media and development of alkaline anion exchange membranes have reinvigorated the search for non-noble metal catalysts for ORR, and revitalized the interest in anion exchange membrane fuel cells (AEMFC) [4–7]. One of the main advantages of AEMFCs over their acidic analogs [8,9] is the availability of effective and inexpensive non-platinum electrocatalysts such as MnO_2 [10,11], nickel [12,13], silver [14,15], cobalt [16,17], and iron [18,19].

The discovery of cobalt phthalocyanine cathodic catalyst by Jasinski [20] was followed by numerous studies of organometallic complexes as promising alternatives for Pt-based electrocatalysts for ORR [21–25]. Among the variety of transition metal macrocycle complex catalysts with different central metal atoms [26] and synthesis methods that have been reported in the literature [24,25], iron- and cobalt-based materials have been identified to exhibit the best activity for ORR under various metal loadings [27–30]. Furthermore, major progress has been reported on metal complex systems reminiscent of enzymes which mimic their coordination environment [31] and proton-coupled electron-transfer process [32–34]. These cofacial porphyrins and related compounds have the basic structure of cytochrome *c* oxidase or related heme/copper terminal oxidases and appear to be the best molecular electrocatalysts with regard to ORR yet found [35,36].

In this paper, we report the results of the evaluation and characterization of a novel carbon-supported bicore CuFe electrocatalyst. The bulk structural and electronic properties of this material were characterized in the context of its kinetics behavior and overall electrochemical performance toward the ORR in an alkaline electrolyte.

2. Experimental

The CuFe/C catalyst was produced on a commercial scale and provided by Acta S.p.A., Italy. The catalyst was synthesized by adsorption of a mixture of iron and copper phthalocyanine-based complexes onto a carbon black support followed by a heat-treatment at 800–900 °C in an Ar atmosphere. A more detailed synthesis procedure can be found in the relevant patent [37]. The metal content of the CuFe/C composite catalyst was determined by ICP-MS (VG Elemental Plasmaquad-2 (PQ2)) to be 1.5 wt.% for Fe and 1.7 wt.% for Cu. The catalyst surface area was 751 $m^2\ g^{-1}$

* Corresponding author. Tel.: +1 510 486 6002; fax: +1 510 486 5454.
E-mail address: R_Kostecki@lbl.gov (R. Kostecki).

0378-7753/$ – see front matter © 2011 Elsevier B.V. All rights reserved.
doi:10.1016/j.jpowsour.2011.04.016

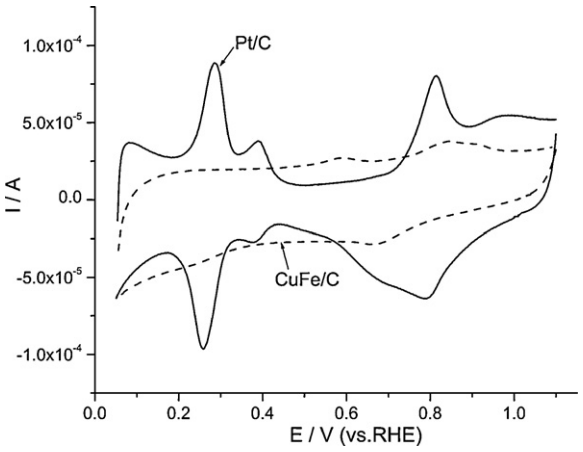

Fig. 1. Cyclic voltammograms of Pt/C and CuFe/C catalysts in Ar-saturated 0.1 M KOH. Scan rate: 50 mV s^{-1}.

as measured with a Micromeritics ASAP 2010 BET system. The surface area of the carbon support used to prepare the catalyst was 1413 m^2 g^{-1}. A commercial Pt/C (30%) catalyst powder was obtained from the BASF Fuel Cell, Inc. and was used for comparative studies. All other chemicals were analytical grade as purchased from Sigma–Aldrich.

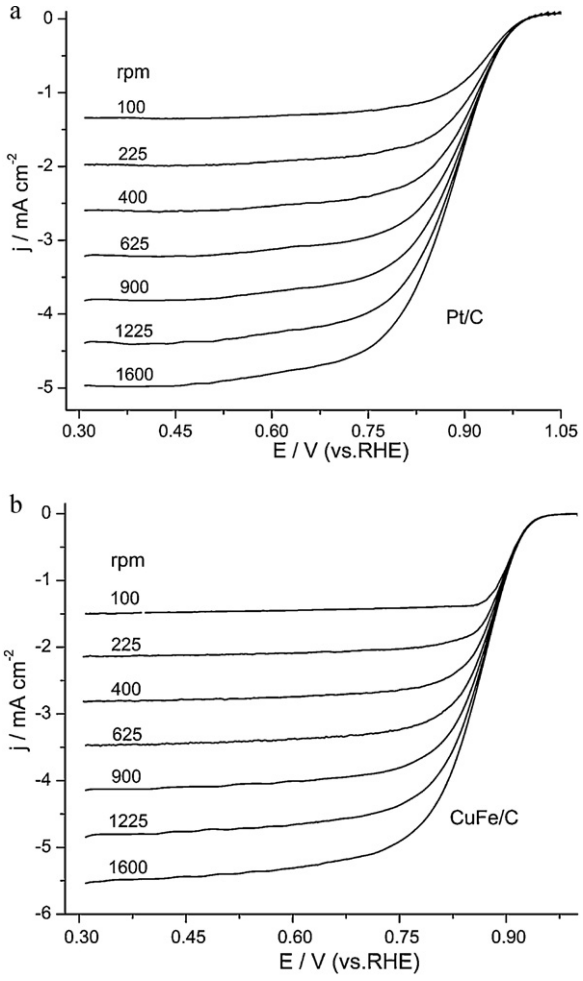

Fig. 2. RDE current density (based on the geometric area of the glassy carbon electrode) at different rotating rates obtained in O_2-saturated 0.1 M KOH on (a) Pt/C and (b) CuFe/C. Scan rate: 20 mV s^{-1}.

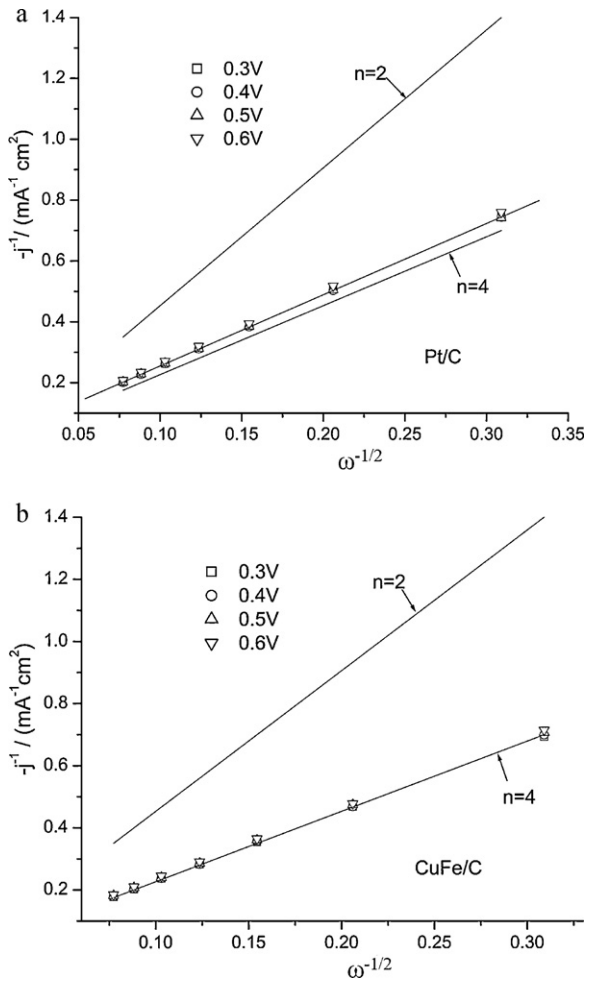

Fig. 3. Koutecky–Levich plots for ORR in O_2-saturated 0.1 M KOH solution at different potentials at (a) Pt/C and (b) CuFe/C.

Composite electrodes were prepared on a glassy carbon disk substrate (5.61 mm dia, Pine Instrument) that was gradually polished with 1.0, 0.3 and 0.05 μm alumina paste (Buehler, Lake Bluff, IL), and then sonicated in distilled water for 5 min. The catalyst inks were prepared by dispersing 0.0368 g of the CuFe/C or 0.0247 g of Pt/C catalyst powders into 20 ml of 2-propanol (HPLC grade, Alfa Aesar) and deionized water (Mega pure, Millipore) (1:1 wt.%) and then sonicating for >30 min to produce a uniform suspension. 10 μL of the catalyst ink was dispersed uniformly on the glassy carbon (GC) substrate and dried at room temperature. The total metal loading was determined to be 2.4 μg cm^{-2} for CuFe/C, and 15 μg cm^{-2} for Pt/C films.

Electrochemical measurements were conducted at room temperature in a standard three-compartment electrochemical cell filled with 0.1 M KOH. All potentials were measured with respect to a reversible hydrogen electrode (RHE) in the same electrolyte. A rotating disk electrode (RDE) setup from Pine Instruments, Inc. was coupled with a Reference 600 potentiostat (Gamry Instruments, Inc.). Cyclic voltammograms and ORR polarization curves of the composite electrodes were recorded in Ar- and O_2-saturated 0.1 M KOH electrolyte.

TEM images of the catalyst powder samples that were ultrasonically dispensed on Cu grid holders were obtained with a JEM-2010 (JEOL Ltd.) microscope, equipped with an INCA Energy TEM 100 EDS analyzer (OXFORD Instruments). An XRD pattern of the CuFe/C catalyst was collected with a Rigaku Ultima III diffractometer, using a Bragg–Brentano geometry and Cu Kα radiation (λ = 1.5418 Å) over

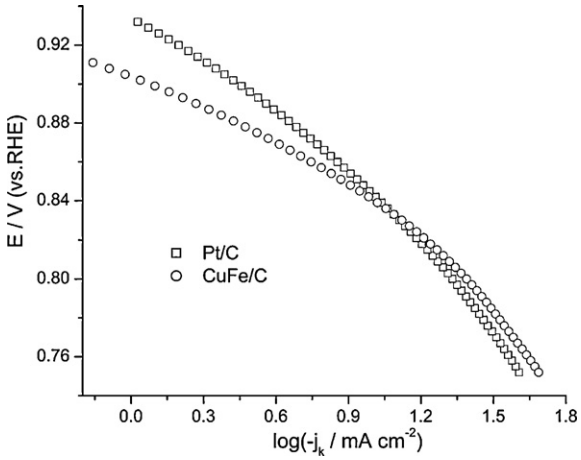

Fig. 4. Tafel plots for ORR obtained from RDE during the anodic sweep at 900 rpm on Pt/C and CuFe/C composite electrodes.

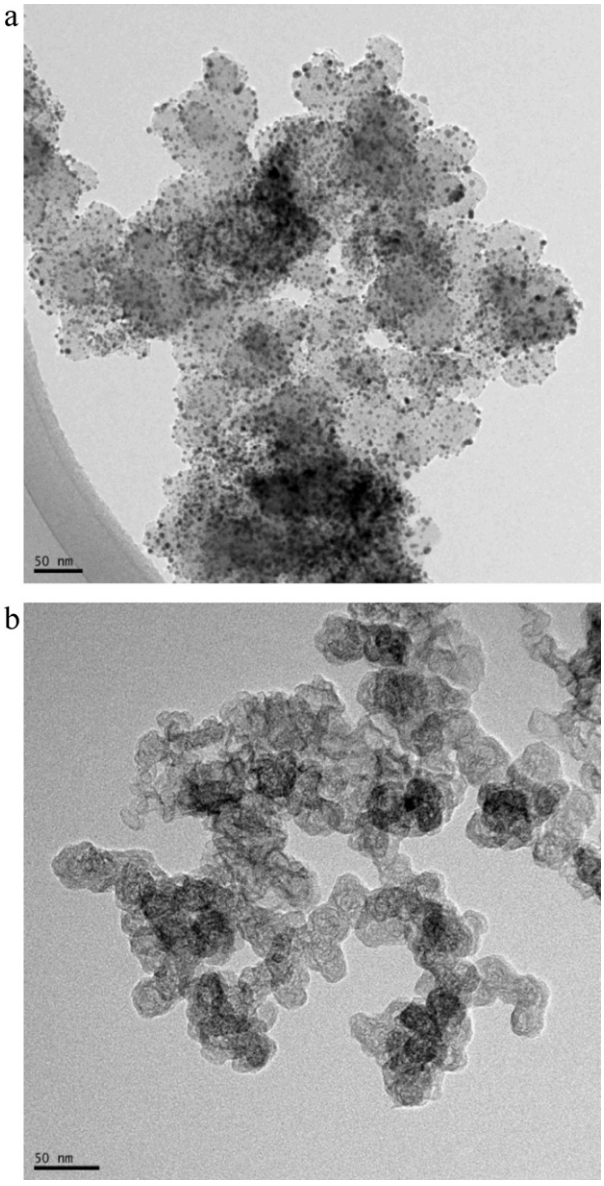

Fig. 5. TEM image of (a) CuFe/C and (b) Pt/C catalyst powders.

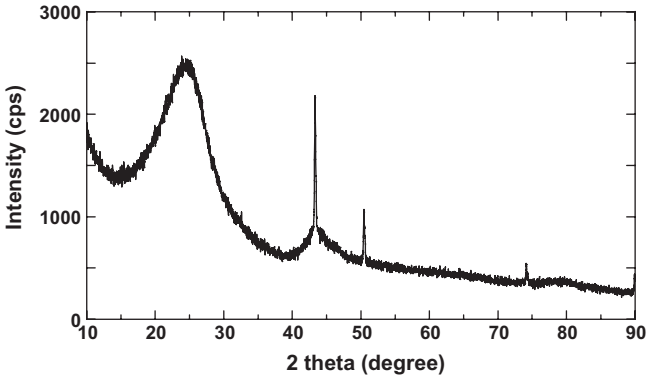

Fig. 6. XRD pattern of the CuFe/C catalyst powder.

a scan range of 10–90° (2θ) at a scan rate of 0.2°/min and resolution of 0.02°.

CuFe/C and other composites were characterized using high resolution X-ray photoelectron spectroscopy (HR-XPS), performed on a VG Scienta ESCA 300 equipped with an 8-kW rotating anode source, a 7-crystal monochromator for Al Kα X-rays ($h\nu$ = 1486.7 eV), and a 300-mm radius hemispherical analyzer with a position-sensitive detector. The measurements were carried out at a take-off angle of 90° with respect to the surface plane of the sample. The analyzer pass energy was set at 300 eV to achieve a resolution of 0.2 eV. Pure Fe(III) meso-tetraphenylporphyrine chloride (Fe(TPP)Cl), Cu metal, and Cu_2O (Sigma–Aldrich) were analyzed to provide reference spectra for Fe2p, Cu2p and N1s core levels. Cu Auger (LMM) spectra were also recorded. All HR-XPS spectra of the CuFe/C composite were referenced to a C1s peak at 284.5 eV binding energy (BE) for carbon black. Curve-fitting was performed with CASA XPS MFC Application software, version 2.3.12.8. A Shirley background was selected to account for inelastic scattering, and all peaks were fitted with a Gaussian/Lorentzian function using a 70/30 ratio. The full-width-at-half-maximum (FWHM) for each of the component peaks was set at 1.0 eV for C1s spectra, 1.5 eV for O1s spectra, 1.1 eV for N1s spectra, and 1.9 eV for Cu2p spectra.

3. Results and discussion

3.1. Electrochemical performance for ORR

Cyclic voltammograms of the Pt/C and CuFe/C electrodes in Ar-saturated 0.1 M KOH are shown in Fig. 1. The Pt/C voltammogram shows typical Pt features, i.e., a hydrogen UPD region between 0.05 V and 0.425 V, followed by a double layer region, and specific adsorption of OH^- on Pt crystal faces at E > 0.75 V [38,39]. The CuFe/C electrode exhibits a large double-layer capacitance current that originates from the underlying pyropolymer and supporting carbon matrix. The anodic peak at 0.58 V can be ascribed to oxidation of quinone and phenol surface groups on the carbon-based pyropolymer backbone. [40,41] The second anodic peak at 0.84 V and the corresponding cathodic peak at 0.68 V can be assigned to redox reactions at central Cu and Fe ions. The low intensity of these peaks is due to extremely low CuFe catalyst loading (ca. 0.75 at.%) as compared to surface modified electrodes [40,42,43].

The RDE scans of the Pt/C and the CuFe/C electrodes in O_2-saturated 0.1 M KOH are shown in Fig. 2a and b, respectively. In both cases, three separate potential regions can be identified: a diffusion-controlled region (E < 0.65 V) is followed by a mixed diffusion-kinetic limited region (0.65V < E < 0.85 V) and a Tafel region (E > 0.85 V). Fig. 3a and b shows Koutecky–Levich $1/j$ vs. $1/\omega^{1/2}$ plots [44] for the Pt/C and the CuFe/C electrodes based

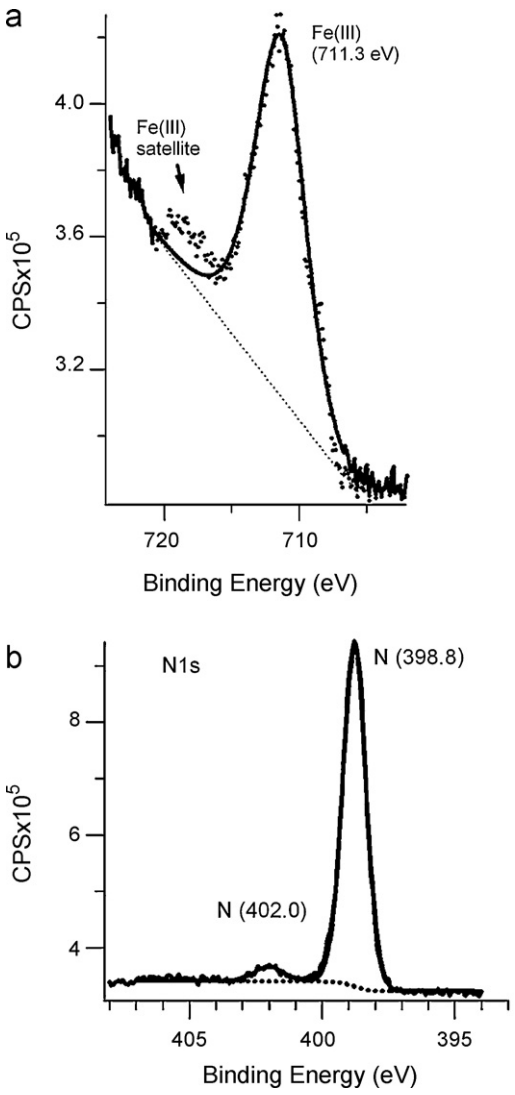

Fig. 7. HR-XPS spectra for Fe(TPP)Cl: (a) $Fe2p_{3/2}$ and (b) N1s.

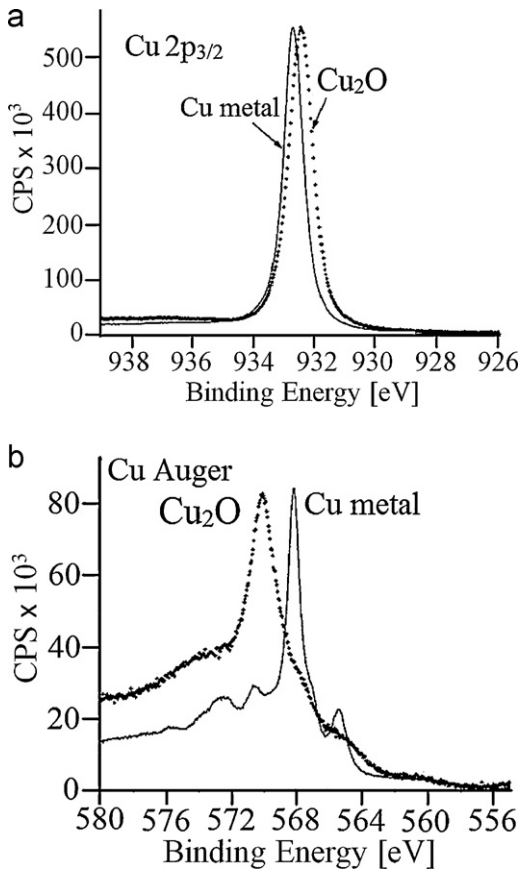

Fig. 8. HR-XPS spectra for Cu and Cu_2O: (a) $Cu2p_{3/2}$ and (b) CuAuger electron region.

on Eqs. (1) and (2) [44]:

$$\frac{1}{j} = \frac{1}{j_k} + \frac{1}{j_d} \tag{1}$$

$$j_d = 0.620nFD^{2/3}C_0\nu^{-1/6}\omega^{1/2} \tag{2}$$

where j_k is the kinetic current density, j_d is diffusion limiting current density, n is the number of exchanged electrons, ω is the angular frequency of rotation, F is the Faraday constant (96485 C mol^{-1}), D is the diffusion coefficient of molecular O_2 in 0.1 M KOH solution (1.9×10^{-5} cm^2 s^{-1}), ν is the kinematic viscosity (1×10^{-2} cm^2 s^{-1}), and C_0 is the concentration of molecular oxygen (1.2×10^{-6} mol cm^{-3}) [45,46]. The theoretical plots for ORR, which correspond to 2 electron and 4 electron processes are shown in the same graph.

The number of exchanged electrons n was calculated from the slope of the experimental plots and are listed in Table 1. A 4-electron charge-transfer ORR process is characteristic of both the Pt/C and CuFe/C electrodes. This indicates the absence of isolated metallic Cu or Fe particles because 3d transition metals tend to produce H_2O_2, an intermediate in oxygen reduction, that cannot be further reduced to H_2O, thereby causing a low n value [47,48].

A comparison of the ORR mass-transport-corrected Tafel kinetics of Pt/C and CuFe/C is shown in Fig. 4, assuming a first-order reaction for oxygen reduction [39,46,49]. These Tafel curves were derived according to the following equation [50,51]:

$$E = E_0 + b\log\frac{j_k}{j_0} \tag{3}$$

where E_0 stands for the equilibrium open-circuit potential (E_0 = 1.229 V vs. RHE under standard conditions), b is the Tafel slope, $j_k = (j\,j_d)/(j_d - j)$ is the kinetics current density, and j_0 is the exchange current density.

The Tafel slopes in the low overpotential range ($E > 0.85$ V) and the high overpotential range ($E < 0.85$ V) on Pt/C and CuFe/C are shown in Table 1. The values obtained agree quite well with those on Pt/C and Fe–phthalocyanine/C under similar conditions [19]. It has been pointed out that the Tafel slopes for ORR are controlled by both "energetic effects" (Temkin, Langmuir adsorption) [52,53] and "blocking effects" (surface coverage of OH controlling O_2 adsorption) [54]. The deviation of the Tafel slope value for CuFe/C from that of Pt/C indicates that the intermediate adsorption on CuFe/C follows a different model. We suggest that the surface coverage of OH controlling the O_2 adsorption on active sites in CuFe/C is higher than that on Pt/C due to the affinity of hydroxyl groups [55,56], which produces a "blocking effect" [54], and consequently a lower kinetic current. The values of mass activity [57] for evaluating the catalytic activity of Pt/C and CuFe/C for ORR are also given in Table 1. Interestingly, the CuFe/C catalyst exhibits equal or higher performance with a 6-fold lower total metal loading compared to Pt/C at typical cathodic operating potentials (0.6–0.85 V) for fuel cells [58,59].

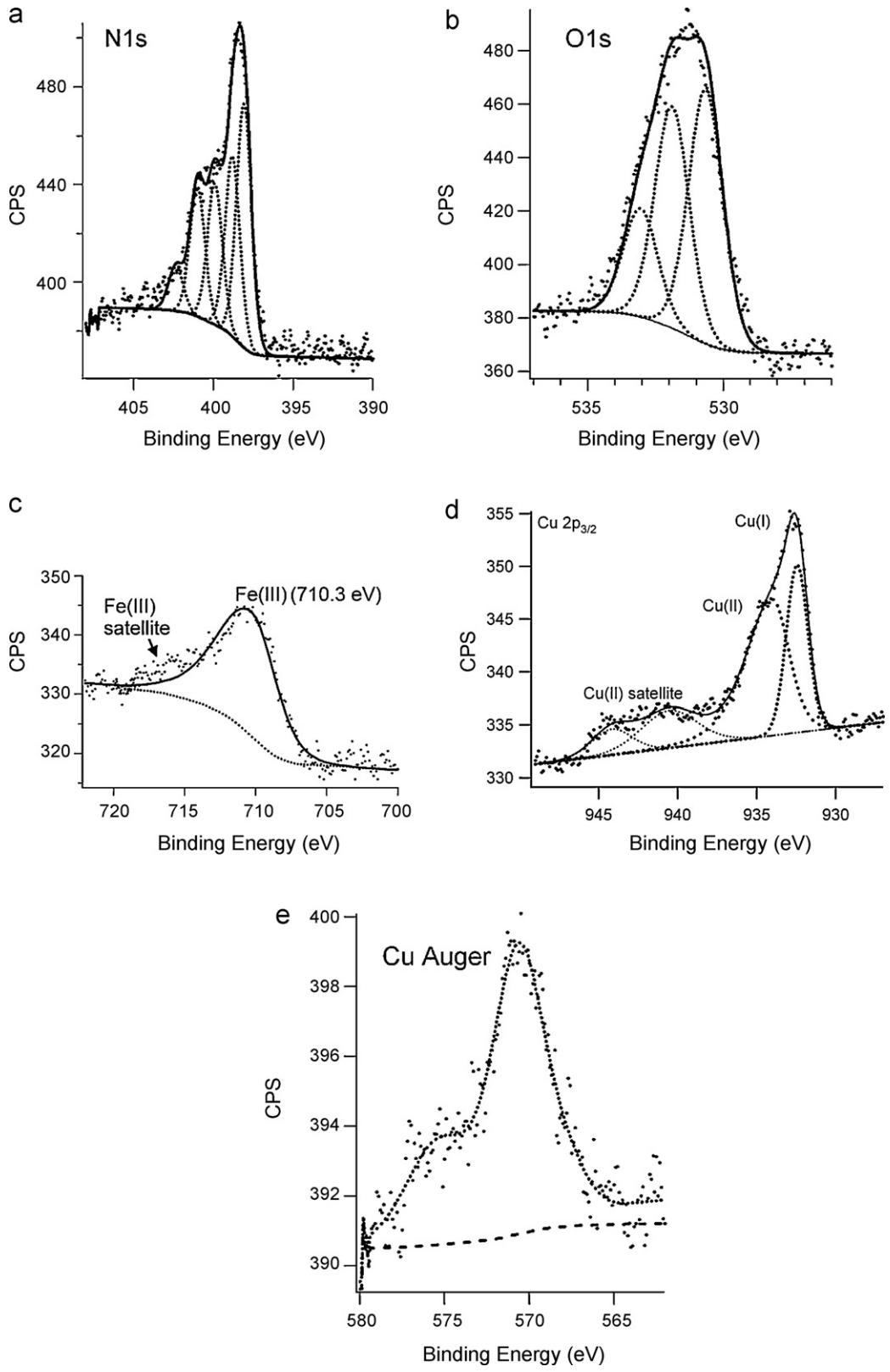

Fig. 9. HR-XPS spectra for the CuFe/C catalyst: (a) N1s, (b) O1s, (c) Fe2$p_{3/2}$, (d) Cu2$p_{3/2}$, and (e) Cu Auger electron region.

3.2. TEM, XRD and HR-XPS characterization

A TEM image of the Pt/C electrocatalyst powder (Fig. 5a) shows 2–5 nm Pt particles which are homogeneously dispersed on the carbon support. Fig. 5b shows a representative TEM image of the CuFe/C electrocatalyst. Large agglomerates of 10–30 nm spherical carbon particles are clearly observed but the supported transition metals are not clearly distinguished in the image. This indicates a very fine dispersion of Cu and Fe in the carbonaceous framework.

Table 1
Electrode kinetic parameters for Pt/C (30%, BASF fuel cells) and CuFe/C catalysts in 0.1 M KOH.

Catalyst	Metal loading on the electrode ($\mu g\,cm^{-2}$)	The number of exchanged electrons (n)	Mass activity ($mA\,cm^{-2}$)			Tafel slope ($mV\,decade^{-1}$)
			@0.90 V	@0.85 V	@0.80 V	
Pt/C (BASF fuel cells)	15	4	2.87	8.61	21.4	130/71
CuFe/C	2.42	4	1.26	7.39	24.5	113/45

An XRD pattern of the CuFe/C composite catalyst powder is shown in Fig. 6. The broad peak centered at 24° originates from disordered graphite (0 0 2) diffraction. The three sharp peaks at 43.32°, 50.46° and 74.14° match closely those from a FeN_x compound (ICSD 01-075-2129). We suggest that the sharp XRD peaks originate from a FeCu–N_x compound in the CuFe/C composite catalyst.

To facilitate HR-XPS analysis of the composite catalyst we recorded spectra of relevant standard reference compounds. The spectrum of the Fe(TPP)Cl compound exhibits a broad Fe $2p_{3/2}$ peak at 711.3 eV (Fig. 7a) and a single N1s peak at 398.8 eV (Fig. 7b). The HR-XPS spectrum of Cu metal and Cu_2O display Cu$2p_{3/2}$ peaks at very similar energies, i.e., 932.4 and 932.7 eV for Cu(0) and Cu(I), respectively (Fig. 8a). The Cu Auger spectra of these two materials offer better energy separation for chemical state indentification (Fig. 8b).

HR-XPS spectra of the N1s, O1s, Fe2p and Cu2p core levels for the CuFe/C catalyst are shown in Fig. 9. The N1s spectra of the CuFe/C catalyst (Fig. 9a) can be deconvoluted into five peaks: 398.0, 398.8, 400.0, 401.0, and 402.4 eV. The N1s peak at 398.0 eV arises from formation of metal nitride compounds. Significantly, we assign the peak at 398.8 eV to N coordinated to Fe in some partially decomposed porphyrin fragment that remains after high temperature annealing. The other N1s peaks arise from more extensive decomposition of the metal phthalocyanines in which N is no longer coordinated to the metal and is bonded in some C_xN_y polymer or compound. The presence of N1s peaks other than that of the nitride indicates that the metal phthalocyanine was not fully decomposed by the high temperature annealing. Retention of metal-nitrogen bonding after heat treatments at 500–700 °C was also observed by Faubert et al. [60] The O1s spectrum of the CuFe/C catalyst (Fig. 9b) can be deconvoluted into three peaks: 530.6, 531.9 and 533.1 eV. The Fe$2p_{3/2}$ peak (Fig. 9c) at 710.3 eV is due to the presence of Fe(III) species. High temperature heat treatment of the catalyst precursors did not cause significant reduction of the Fe(III) sites. The 1.0 eV shift to low binding energy of the Fe$2p_{3/2}$ peak from 711.3 eV in Fe(TPP)Cl indicates a higher electron density environment at the Fe(III) sites. The CuFe/C catalyst is characterized by two Cu$2p_{3/2}$ peaks at 932.7 and 934.8 eV (Fig. 9d). The 934.8 eV peak corresponds to Cu(II), and the satellite peak at higher BE (940–945 eV) confirms the existence of Cu(II) compounds. These peaks are possibly due to $Cu(OH)_2$, since CuO has a Cu$2p_{3/2}$ peak at 933.6 eV. To resolve the Cu oxidation state of the lower BE peak at 932.7 eV, we examined CuAuger spectrum (Fig. 9e). The strong peak at 570 eV and the absence of any peak at 568 eV indicates the presence of Cu(I) species. Although the existence of Cu_2O cannot be excluded at this stage, Cu(I) in an organic complex framework with a N_1 ligand attached is a reasonable assignment. The conclusions from HR-XPS are consistent with the electrochemical results that indicate no presence of metallic Cu or Fe.

A plausible working mechanism of the CuFe/C catalyst for ORR is illustrated in Fig. 10. The reaction mechanism may involve a combined effect from Fe and Cu where N_xFe(III) serves as the ORR active site and Cu(I)/Cu(II) serves as the redox mediator during ORR. We suggest that the rate determining step is an inner-sphere electron transfer that leads to an adduct formation between Fe–N_x with O_2 [61,62]. The Cu(II)/Cu(I) redox mediator may carry electron from the electrode to the catalyst sites and accelerate the reduction of the adduct.

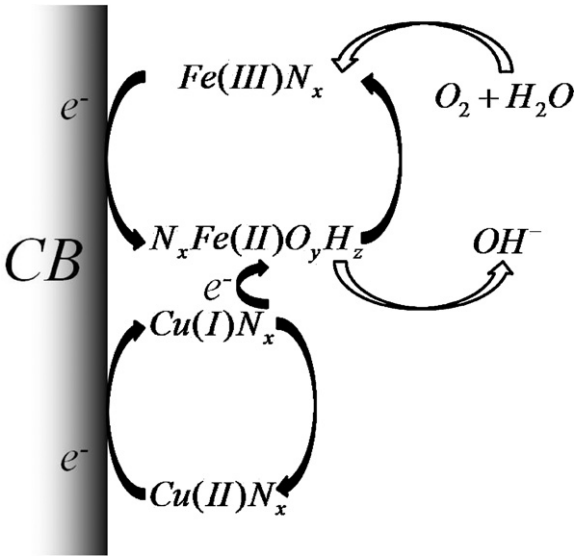

Fig. 10. A diagram of an operating mechanism for the ORR for CuFe/C catalyst.

4. Conclusions

A novel commercial CuFe/C ORR catalyst that was synthesized from a mixture of iron and copper phthalocyanine-based complexes was evaluated and characterized in an alkaline electrolyte. RDE experiments demonstrated that this non-noble metal electrode material exhibits similar catalytic activity for ORR as a standard Pt/C material at 6-fold less metal loading. HR-XPS measurements showed that the CuFe/C composite powder contains N_xFe(III) and Cu(II)/Cu(I) compounds. We propose a catalyst operation mechanism in which N_xFe(III) serves as the active site for ORR and the Cu(II)/Cu(I) redox mediator works as the electron shuttle from the electrode to the catalyst-oxygen (N_xFe–O_2) adduct. Such a catalyst-mediator combination can be used as a novel strategy to design efficient non-noble catalysts for electroreduction of O_2.

Acknowledgements

This work was supported by the Assistant Secretary for Energy Efficiency and Renewable Energy, Office of Hydrogen, Fuel Cells and Infrastructure Technologies of the U.S. Department of Energy under Contract No. DE-AC02-05CH11231. Part of this work was supported by the National Science Foundation under Grant No. 0616644. The authors would like to thank Dr. Agustín Bueno Lopez for assistance with the TEM experiments.

References

[1] T. Burchardt, J.H. Miners, P. Gouerec, W. Stinissen, Prepr. Symp. Am. Chem. Soc., Div. Fuel Chem. 46 (2001) 473–474.
[2] E.D. Geeter, M. Mangan, S. Spaepan, W. Stinissen, G. Vennekens, J. Power Sources 80 (1999) 207–212.

[3] G.F. McClean, T. Niet, S. Prince-Richard, N. Djilali, Int. J. Hydrogen Energy 27 (2002) 507–526.
[4] R.C.T. Slade, Abstracts of Papers 234th ACS National Meeting, Boston, MA, United States, August 19–23, 2007 (FUEL-042).
[5] R.C.T. Slade, J.R. Varcoe, Prepr. Symp. Am. Chem. Soc., Div. Fuel Chem. 52 (2007) 319–320.
[6] J.R. Varcoe, R.C.T. Slade, Electrochem. Commun. 8 (2006) 839–843.
[7] G. Wang, Y. Weng, D. Chu, R. Chen, D. Xie, J. Membr. Sci. 332 (2009) 63–68.
[8] J.R. Varcoe, R.C.T. Slade, Fuel Cells 5 (2005) 187–200.
[9] R.C.T. Slade, J.R. Varcoe, Solid State Ionics 176 (2005) 585–597.
[10] F. Cheng, Y. Su, J. Liang, Z. Tao, J. Chen, Chem. Mater. 22 (2010) 898–905.
[11] I. Roche, K. Scott, J. Electroanal. Chem. 638 (2010) 280–286.
[12] G.M. Swain, B.J. Tatarchuk, Proc. Electrochem. Soc. 94 (4) (1994) 237–248.
[13] R. Yang, K. Stevens, J.R. Dahn, J. Electrochem. Soc. 155 (2007) B79–B91.
[14] J. Guo, A. Hsu, D. Chu, R. Chen, J. Phys. Chem. C 114 (2010) 4324–4330.
[15] G.K.H. Wiberg, K.J.J. Mayrhofer, M. Arenz, Fuel Cells (Weinheim, Germany) 10 (2010) 575–581.
[16] T.S. Olson, S. Pylypenko, P. Atanassov, K. Asazawa, K. Yamada, H. Tanaka, J. Phys. Chem. C 114 (2010) 5049–5059.
[17] Y. Wang, D. Zhang, H. Liu, J. Power Sources 195 (2010) 3135–3139.
[18] R. Baker, D.P. Wilkinson, J. Zhang, ECS Trans. 16 (2009) 43–61.
[19] R. Chen, H. Li, D. Chu, G. Wang, J. Phys. Chem. C 113 (2009) 20689–20697.
[20] R.J. Jasinski, Nature (London, U.K.) 201 (1964) 1212–1213.
[21] C.W.B. Bezerra, L. Zhang, K. Lee, H. Liu, A.L.B. Marques, E.P. Marques, H. Wang, J. Zhang, Electrochim. Acta 53 (2008) 4937–4951.
[22] C.W.B. Bezerra, L. Zhang, K. Lee, H. Liu, J. Zhang, Z. Shi, A.L.B. Marques, E.P. Marques, S. Wu, J. Zhang, Electrochim. Acta 53 (2008) 7703–7710.
[23] B. Wang, J. Power Sources 152 (2005) 1–15.
[24] Y. Feng, N. Alonso-Vante, Phys. Status Solidi B 245 (2008) 1792–1806.
[25] L. Zhang, J. Zhang, D.P. Wilkinson, H. Wang, J. Power Sources 156 (2006) 171–182.
[26] D. Chu, R. Jiang, Solid State Ionics 148 (2002) 591–599.
[27] M. Bron, S. Fiechter, M. Hilgendorff, P. Bogdanoff, J. Appl. Electrochem. 32 (2002) 211–216.
[28] H. Wang, R. Cote, G. Faubert, D. Guay, J.P. Dodelet, J. Phys. Chem. B 103 (1999) 2042–2049.
[29] M. Lefevre, J.P. Dodelet, P. Bertrand, J. Phys. Chem. B 104 (2000) 11238–11247.
[30] M. Lefevre, J.P. Dodelet, P. Bertrand, J. Phys. Chem. B 106 (2002) 8705–8713.
[31] J.P. Collman, N.K. Devaraj, R.A. Decreau, Y. Yang, Y.-L. Yan, W. Ebina, T.A. Eberspacher, C.E.D. Chidsey, Science (Washington, DC, USA) 315 (2007) 1565–1568.
[32] C.J. Chang, L.L. Chng, D.G. Nocera, J. Am. Chem. Soc. 125 (2003) 1866–1876.
[33] C.J. Chang, Z.-H. Loh, C. Shi, F.C. Anson, D.G. Nocera, J. Am. Chem. Soc. 126 (2004) 10013–10020.
[34] C.J. Chang, Y. Deng, D.G. Nocera, C. Shi, F.C. Anson, C.K. Chang, Chem. Commun. (Cambridge) (2000) 1355–1356.
[35] J.P. Collman, R. Boulatov, C.J. Sunderland, in: K.M. Kadish, K.M. Smith, R. Guilard (Eds.), The Porphyrin Handbook, Academic Press, Boston, 2003.
[36] J.P. Collman, P.S. Wagenknecht, J.E. Hutchison, Angew. Chem. Int. Ed. 33 (1994) 1525–1674.
[37] S. Catanorchi, M. Piana, Acta S.p.A., Italy, Application: WO, 2009, Chemical Indexing Equivalent to 151:452785 (EP), p. 31.
[38] Q. He, W. Chen, S. Mukerjee, S. Chen, F. Laufek, J. Power Sources 187 (2009) 298–304.
[39] L. Genies, Y. Bultel, R. Faure, R. Durand, Electrochim. Acta 48 (2003) 3879–3890.
[40] R. Baker, D.P. Wilkinson, J. Zhang, Electrochim. Acta 53 (2008) 6906–6919.
[41] S. Dong, J. Ding, Synth. Met. 24 (1988) 273–281.
[42] R. Baker, D.P. Wilkinson, J. Zhang, Electrochim. Acta 54 (2009) 3098–3102.
[43] A. Van der Putten, A. Elzing, W. Visscher, E. Barendrecht, J. Electroanal. Chem. Interfacial Electrochem. 221 (1987) 95–104.
[44] E. Higuchi, H. Uchida, M. Watanabe, J. Electroanal. Chem. 583 (2005) 69–76.
[45] R.E. Davis, G.L. Horvath, C.W. Tobias, Electrochim. Acta 12 (1967) 287–297.
[46] K. Vaik, A. Sarapuu, K. Tammeveski, F. Mirkhalaf, D.J. Schiffrin, J. Electroanal. Chem. 564 (2004) 159–166.
[47] E.M. Crabb, R. Marshall, D. Thompsett, J. Electrochem. Soc. 147 (2000) 4440.
[48] U.A. Paulus, A. Wokaun, G.G. Scherer, T.J. Schmidt, V. Stamenkovic, N.M. Markovic, P.N. Ross, Electrochim. Acta 47 (2002) 3787–3798.
[49] M.L. Calegaro, F.H.B. Lima, E.A. Ticianelli, J. Power Sources 158 (2006) 735–739.
[50] Q. He, S. Mukerjee, R. Zeis, S. Parres-Esclapez, M.J. Illan-Gomez, A. Bueno-Lopez, Appl. Catal. A 381 (2010) 54–65.
[51] S. Baranton, C. Coutanceau, C. Roux, F. Hahn, J.M. Leger, J. Electroanal. Chem. 577 (2005) 223–234.
[52] F.H.B. Lima, M.J. Giz, E.A. Ticianelli, J. Braz. Chem. Soc. 16 (2005) 328–336.
[53] M.T. Giacomini, E.A. Ticianelli, J. McBreen, M. Balasubramanianb, J. Electrochem. Soc. 148 (2001) A323–A329.
[54] N.M. Markovic, T.J. Schmidt, V. Stamenkovic, P.N. Ross, Fuel Cells 1 (2001) 105–116.
[55] H. Liu, Y. Wei, Y. Sun, W. Wei, Colloids Surf. A 252 (2005) 201–205.
[56] O. Bekaroglu, J. Porphyrins Phthalocyanines 4 (2000) 465–473.
[57] E. Antolini, J.R.C. Salgado, M.J. Giz, E.R. Gonzalez, Int. J. Hydrogen Energy 30 (2005) 1213–1220.
[58] W. Vielstich, A. Lamm, H.A. Gasteiger, Handbook of Fuel Cells: Fundamentals, Technology, Applications, Wiley, 2003.
[59] R.A. Sidik, J. Solid State Electrochem. 13 (2009) 1123–1126.
[60] G. Faubert, G. Lalande, R. Cote, D. Guay, J.P. Dodelet, L.T. Weng, P. Bertrand, G. Denes, Electrochim. Acta 41 (1996) 1689–1701.
[61] G. Wei, J.S. Wainright, R.F. Savinell, J. New Mater. Electrochem. Syst. 3 (2000) 121–129.
[62] A.B. Anderson, R.A. Sidik, J. Phys. Chem. B 108 (2004) 5031–5035.